Paste 2026 – AB Fourie, M Horta, M Oliveira & S Wilson (eds)

doi:10.36487/ACG_repo/2655_36

A robust numerical framework for non-Newtonian tailings flows in dam breach scenarios

Nadia Skifa [a,*], James McKenna [a], Vassilis Glenis [a]

[a] *School of Civil and Geospatial Engineering, Newcastle University, UK*

Abstract

Tailings storage facilities (TSF) are among the largest man-made infrastructures, and their failures lead to devastating consequences. Understanding the flow of tailings following a dam breach is critical for designing effective mitigation strategies to protect downstream communities, and ecosystems. However, commonly applied flow models often struggle to capture the complex non-Newtonian behaviour of tailings, particularly the variation in viscosity under rapidly evolving flow conditions. To overcome this limitation, this work presents a finite-volume shock-capturing solver for the incompressible flow equations, incorporating a quadratic viscoplastic rheology to model tailings flows. In addition, the model integrates robust hydrodynamic reconstruction techniques to ensure the balance of fluxes, material interfaces, and nonlinear flow dynamics. By incorporating a more-realistic representation of the yield and viscous behaviour of tailings, the model addresses key limitations in existing approaches and significantly improves physics-based modelling. The resulting numerical model proved stable and robust for benchmark and idealised dam breach scenarios. In this paper, the development of the scheme is outlined, its numerical performance is discussed and results from the benchmark and idealised dam breach scenarios are presented. This approach represents advancements in tailings flow simulation, offering improved predictive capabilities for both research applications and operational dam safety assessments.

Keywords: *tailings storage facilities, tailings flow modelling, Riemann solver, non-Newtonian flow*

1 Introduction

The global demand for metals and minerals continues to accelerate, driving an unprecedented expansion of mining activity worldwide (Newland Bowker & Chambers 2015). With this growth comes a parallel increase in the volume of mining waste, stored in stages throughout the operational life of the mine. Tailings storage facilities (TSF) rank among the world's largest embankment structures, making their stability critical. However, the failure rate of these dams has been estimated to be 2 orders of magnitude higher than that of conventional water dams (Azam & Li 2010; Piciullo et al. 2022). When such failures occur, the sudden release of tailings causes catastrophic loss of life, severe ecological damage, and long-term contamination of waterways (Motsau et al. 2022; Rana et al. 2021; Zhu et al. 2024).

Understanding tailings flow dynamics is therefore crucial to effective risk assessment and emergency planning. However, tailings dam failures are fundamentally different from traditional dam failures. They are classified as non-Newtonian flows, in which the viscosity of the tailings varies with shear rate and stress, exhibiting a behaviour that changes in time. This means that during a dam breach, flow resistance evolves continuously with changing stress and shear conditions, producing a complex interplay between yielding, flow acceleration, and deposition. As described by (Coussot 2017), many tailings exhibit viscoplastic behaviour, characterised by a finite yield stress that must be exceeded before flow begins, followed by shear thinning as the material structure breaks down under deformation.

[*] Corresponding author. Email address: N.skifa2@newcastle.ac.uk

Existing numerical approaches for tailings dam break simulation can broadly be classified into 3 categories, each addressing only part of the physical and numerical challenges inherent to tailings flows. Many engineering and commercial models, such as FLO-2D and HEC-RAS, are formulated within the shallow-water equations framework and incorporate viscoplastic rheological formulations to account for non-Newtonian effects (O'Brien & Julien 1988; O'Brien et al. 1993; Brunner 2016; FLO-2D Software Inc. 2004). However, these models typically rely on low-order, relatively diffusive numerical schemes originally developed for surface water flooding applications which limits their ability to resolve sharp hydraulic fronts, wet–dry transitions, and steep gradients in velocity and flow depth that arise as tailings decelerate and progressively deposit. As a result, such models may reproduce the overall inundation footprint but often overestimate runout distances and underestimate depositional thicknesses, as they inadequately capture the strong shear-rate-dependent viscosity increase and momentum loss characteristic of viscoplastic tailings (Kheirkhah Gildeh et al. 2021; Lyu et al. 2019; Kheirkhah Gildeh et al. 2024).

In contrast, granular-flow solvers like RAMMS, DAN3D, and TITAN2D employ robust shock-capturing techniques capable of resolving steep fronts and discontinuities (Kheirkhah Gildeh et al. 2021; Lyu et al. 2019; Kheirkhah Gildeh et al. 2024) yet are based on purely frictional rheologies that neglect viscous and rate-dependent effects. These assumptions restrict their applicability to dry granular or debris-flow regimes and make them unsuitable for hyperconcentrated or slurry-like tailings, where rheological transitions govern flow arrest and deposition. This limitation is evident in several recent studies (Ghahramani et al. 2024; Kheirkhah Gildeh et al. 2024; Wang et al. 2020) where models reproduced the general inundation footprint but failed to represent the depositional behaviour of tailings. These simplifying assumptions are unsuitable for tailings, which behave as non-Newtonian, viscoplastic materials that rapidly lose momentum and deposit as shear rate decreases, and the material 'loses flowability'. In contrast to Newtonian fluids, tailings flows tend to form steep fronts and deposit progressively as they travel, creating sharp gradients in velocity and depth that cannot be captured by Newtonian hydrodynamic models.

Therefore, a critical gap remains, one that this study addresses by posing the following question:

> *"How can we numerically simulate tailings dam break flows in a way that captures their nonlinear, viscoplastic behaviour without sacrificing numerical stability and resolution of sharp fronts?"*

To bridge this gap, we propose a finite-volume, shock-capturing numerical solver for the 2D incompressible flow equations that explicitly incorporates a quadratic viscoplastic rheology. This formulation extends beyond Newtonian approaches by including a shear term that represents yield, viscous, and turbulent-dispersive stresses governing tailings motion. The solver resolves the local Riemann problem at each cell interface of the computational grid, ensuring accurate flux evaluation and stable capture of sharp flow discontinuities. Additionally, the model integrates a hydrodynamic reconstruction of the bed elevation to account for steep or irregular topography to maintain moving equilibria (Berthon & Michel-Dansac 2024).

In this paper, we first present the mathematical and numerical implementation of the solver, then test it against benchmark dam break tests, including both Newtonian and non-Newtonian conditions.

2 Numerical model

2.1 Mathematical formulation

Tailing flows are commonly represented by hyperconcentrated mudflows, characterised by a concentration by volume between 20 and 55% according to (O'Brien et al. 1985) and later reformulated in a depth-averaged shallow-water framework by Julien & Lan (1991) and O'Brien et al. (1993). To better capture the behaviour of such flows, a quadratic viscoplastic rheological model is adopted. This approach effectively incorporates both yield stress and viscous effects and has been widely applied in mudflows and tailings dam breach analyses.

The flow dynamics are governed by the 2D depth-averaged incompressible flow equations, expressed in conservative form as:

$$\frac{\partial U}{\partial t} + \frac{\partial F}{\partial x} + \frac{\partial G}{\partial y} = S(U) \tag{1}$$

$$U = \begin{bmatrix} h \\ hu \\ hv \end{bmatrix}; F = \begin{bmatrix} hu \\ hu^2 + \frac{1}{2}gh^2 \\ huv \end{bmatrix}; G = \begin{bmatrix} hv \\ huv \\ hv^2 + \frac{1}{2}gh^2 \end{bmatrix}; S = \begin{bmatrix} 0 \\ -gh(\frac{\partial Z}{\partial x} + S_{fx}) \\ -gh(\frac{\partial Z}{\partial y} + S_{fy}) \end{bmatrix} \tag{2}$$

Herein, *U* is the vector of conserved variables, *F* and *G* are the vectors of fluxes, and *S* is the vector of sources.

where:

- h = flow depth
- u and v = depth-averaged velocities in x and y directions
- g = gravitational acceleration
- Z = bed elevation
- S_{fx} and S_{fy} = the friction source terms in the x and y directions respectively.

The friction source terms describe the shear stress model arising from the interaction between the tailings particles. The quadratic shear stress model is modelled as the sum of the yield, viscous and turbulent-dispersive stresses (O'Brien et al. 1985):

$$\tau = \tau_\gamma + \tau_V + \tau_{TD}$$

These terms yield the quadratic shear stress model, where yield stress τ_γ includes both cohesive and frictional contributions:

$$\tau = \tau_\gamma + \eta \frac{du}{dy} + C \left(\frac{du}{dy}\right)^2 \tag{3}$$

where:

- du/dy = shear rate
- η = dynamic viscosity that represents the resistance parameter. This parameter varies implicitly both spatially and temporally with shear rate, and should not be interpreted as a constant apparent viscosity in the Newtonian sense.
- C = inertial shear stress coefficient, defined using the mixture density and a representative particle diameter derived from the particle distribution of the tailings mixture.

This formulation effectively describes the combined effects of yield, viscous, and turbulent stresses and has been successfully applied in debris-flow and tailings breach simulations (Ghahramani et al. 2020).

Building on the conceptual framework of depth-integrated shear stress and sediment transport theory, (O'Brien et al. 1993) formulated a dimensionless friction slope (S_{fx}) to represent the total energy losses in the flow:

$$S_f = \frac{\tau_\gamma}{\gamma_m h} + \frac{\eta k u}{8\gamma_m h^2} + \frac{n_d{}^2 |u| u}{h^{4/3}} \tag{4}$$

Here, $\gamma_m = g\rho_m$ is the specific weight of the sediment–water mixture, and k is the laminar flow resistance parameter.

The model includes empirical relationships for yield stress (τ_y) and dynamic viscosity (η). These relationships are derived from rheological testing using rheometers, where τ_y and η are measured as functions of volumetric concentration (C_v) for specific tailings or debris-flow materials. They are valuable when rheological analysis of the tailings material is unavailable:

$$\tau_\gamma = \alpha_1 e^{\beta_1 C_v} \tag{5}$$

$$\eta = \alpha_2 e^{\beta_2 C_v} \tag{6}$$

where α_1, β_1, α_2 and β_2 are coefficients derived from rheological testing using rheometers (O'Brien & Julien 1988).

The coefficient n_d is defined as a function of the Manning's roughness (n):

$$n_d = 0.0538\, n\, e^{6.0896\, C_v} \tag{7}$$

The quadratic rheological formulation thus provides a robust balance between physical accuracy and computational efficiency, making it particularly suitable for modelling the nonlinear behaviour of tailings flows across a wide range of concentrations and flow conditions.

2.2 Numerical solution

The governing equations are solved using a first-order finite-volume, shock-capturing Godunov-type scheme (Godunov 1959). This approach integrates the quadratic viscoplastic rheology and accurately handles source terms, making it well-suited for capturing sharp gradients and discontinuities inherent in dam breach and debris-flow problems (Glenis et al. 2018).

In the Godunov framework, conservative variables are assumed to be piecewise constant within each computational cell at every time step (Toro 2001). The interfaces between cells define local Riemann problems (Harten 1983), whose solutions govern the temporal evolution of the conserved variables. Figure 1 defines the 2D computational domain, where the flow convention is left-to-right in the x direction and bottom to top in the y direction.

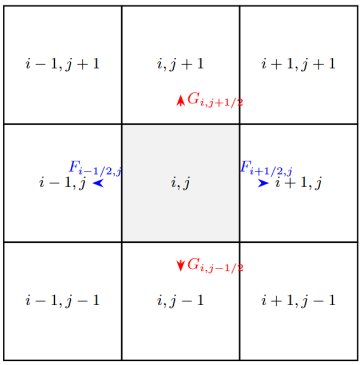

Figure 1 Finite-volume grid showing cell (i, j) linked in all directions with fluxes F (horizontal) and G (vertical)

The generalised Osher–Solomon Riemann solver is implemented to compute intercell fluxes. The numerical fluxes across cell interfaces are expressed as:

$$F_{i+\frac{1}{2},j} = \frac{1}{2}[F(U_L) + F(U_R)] - \frac{1}{2}\int_{U_L}^{U_R} |A(U)| dU_x \tag{8}$$

$$G_{i,j+\frac{1}{2}} = \frac{1}{2}[G(U_B) + G(U_T)] - \frac{1}{2}\int_{U_B}^{U_T} |B(U)| dU_y \tag{9}$$

where, U_L and U_R are the left and right states respectively, and $A = \frac{\partial F}{\partial U}$ and $B = \frac{\partial G}{\partial U}$ are the Jacobian matrices.

The eigenvalues of $A(U)$ and $B(U)$ correspond to the characteristic wave speeds:

$$\lambda_{1x} = u - c\,, \qquad \lambda_{2x} = u\,, \qquad \lambda_{3x} = u + c$$
$$\lambda_{1y} = v - c\,, \qquad \lambda_{2y} = v\,, \qquad \lambda_{3y} = v + c \tag{10}$$

where:

c = wave celerity expressed by $\sqrt{gh}$.

The integrals in the numerical flux are evaluated using Gauss–Legendre quadrature (Dumbser & Toro 2010), expressed as Equations (11) and (12):

$$\int_{U_L}^{U_R} |A(U)|dU_x \approx \frac{U_R - U_L}{2} \sum_{i=1}^{n} w_i |A(U(\xi_i))| \tag{11}$$

$$\int_{U_B}^{U_T} |B(U)|dU_y \approx \frac{U_T - U_B}{2} \sum_{i=1}^{n} w_i |B(U(\xi_i))| \tag{12}$$

For a three-point Gauss quadrature, the integration points and weights are:

- Quadrature points : $\xi_1 = -\sqrt{\frac{3}{5}}\,, \xi_2 = 0\,, \xi_3 = \sqrt{\frac{3}{5}}$
- Weights: $w_1 = w_3 = \frac{5}{9}\,, w_2 = \frac{8}{9}$

The three-point integral method is a simple yet effective calculation with only eigenvalues of the hyperbolic system.

The conserved variables are updated at each time step following the Eq. (13):

$$U_{i,j}{}^{n+1} = U_{i,j}{}^{n} - \frac{\Delta t}{\Delta x}\left(F_{i+\frac{1}{2},j} - F_{i-\frac{1}{2},j}\right) - \frac{\Delta t}{\Delta y}\left(G_{i,j+\frac{1}{2}} - G_{i,j-\frac{1}{2}}\right) + \Delta t S_{i,j}{}^{n} \tag{13}$$

The time step Δt is constrained by the Courant–Friedrichs–Lewy (CFL) stability condition in Eq. (14):

$$\Delta t = \frac{CFL \min(\Delta x, \Delta y)}{\max(|u| + c, |v| + c)} \tag{14}$$

The hydrodynamic reconstruction technique is applied to ensure non-negative water depths and physically consistent interface values (Berthon & Michel-Dansac 2024). The reconstructed depth and discharge at the cell interfaces are given by the set of Equations (15):

$$\begin{cases} h^n_{i+\frac{1}{2},L} = \max\left(0, h_i{}^n + \left(Z_i - Z_{i+\frac{1}{2}}\right) + 2Fr^2\left(h^n_i, h^n_{i+\frac{1}{2}}, q^n_i\right)\mathcal{H}\left(h^n_i, h^n_{i+\frac{1}{2}}, q^n_i, Z_{i+\frac{1}{2}} - Z_i\right)\right) \\ h^n_{i+\frac{1}{2},R} = \max\left(0, h_{i+1}{}^n + \left(Z_{i+1} - Z_{i+\frac{1}{2}}\right) + 2Fr^2\left(h^n_{i+1}, h^n_{i+\frac{1}{2}}, q^n_{i+1}\right)\mathcal{H}\left(h^n_{i+1}, h^n_{i+\frac{1}{2}}, q^n_{i+1}, Z_{i+\frac{1}{2}} - Z_{i+1}\right)\right) \\ q^n_{i+\frac{1}{2},L} = q^n_i \\ q^n_{i+\frac{1}{2},R} = q^n_{i+1} \end{cases} \tag{15}$$

where:

F_r = Froude number

$H(\cdot)$ = hydrodynamic reconstruction function.

While the quadratic rheological model is already established, the model integrates it into a Godunov finite-volume framework (f), with a robust Osher-type Riemann solver that preserves front sharpness and internal flow structure, which is essential for accurately predicting runout distances and arrival times. In addition, the use of hydrodynamic bed reconstruction ensures the well-balanced treatment of bed slopes over irregular terrain, maintaining physical consistency and numerical stability.

3 Model application and set-up

To assess the performance and robustness of the proposed numerical model, 2 simulations were conducted. A series of idealised dam break test cases were set up to verify the model's ability to reproduce well-established benchmark solutions, including the rapid propagation of a mudflow column collapse and the transition between subcritical and supercritical flow regimes (Bagnold 1954). These tests are essential to confirm the scheme's capacity to handle sharp discontinuities and to evaluate numerical stability and mass conservation under varying rheological and topographic conditions. Four benchmark tests were implemented following well-established dam break configurations from the literature, as described below:

- Newtonian flow with Manning friction
- Newtonian flow without friction
- non-Newtonian flow of low viscosity tailings of Glenwood 1
- non-Newtonian flow of high-density tailings of Aspen Pit 1.

The frictionless Newtonian case represents the inviscid shallow-water equations, solely used to verify the numerical scheme against exact Riemann solutions before introducing frictional and rheological dissipation. This case is not intended to represent a physically realistic scenario.

The model's ability to capture the influence of rheology on flow dynamics is assessed using 2 representative non-Newtonian test cases: Glenwood 1 and Aspen Pit 1. Their parameters are derived from the widely used debris-flow rheology of O'Brien & Julien (1988) as implemented in the FLO-2D model. These parameter sets represent empirical rheological characterisations developed through field observations and back-analysis of debris-flow behaviours in Glenwood Canyon, Colorado, and the Aspen area, USA. The quadratic parameters were then defined by O'Brien & Julien (1988) by matching observed runout, velocity, and deposition patterns using FLO-2D, supported by laboratory testing of sediment samples to constrain concentration and particle properties.

Although not specific to mine tailings, these parameter sets represent typical concentrated sediment–water mixtures and provide useful rheological benchmarks to tailings flow modelling. However, for application to specific tailings dams, the rheological parameters should be determined through laboratory testing of tailings samples. In the absence of site-specific measurements, these parameter sets provide representative values for model testing (Rico 2008).

A 2D rectangular grid domain n_x and n_y of 10 × 10 m (Δx = Δy = 1.0 m) was initialised with closed boundaries. The bottom elevation $z_b(x,y)$ is prescribed as a bilinear planar slope descending along both coordinate directions, defined numerically as:

$$z_b(i,j) = 0.02(n_x - i) + 0.02\big(n_y - j\big) \tag{16}$$

A reservoir of initial depth h = 5.0 m was defined over the first quarter of the domain as shown in Figure 2, representing a dam break over a dry bed. The left and right states of the Riemann problem were initialised as:

$$\begin{cases} h_L = 5.0\,m\,, \; u_L = 0.0 \;\; m/s \\ h_R = 0.0\,m\,, \; u_L = 0.0\,m/s \end{cases} \tag{17}$$

Each of the 4 cases was run for t = 20 s to capture the front propagation of the wave over sloping topography, with a Courant number of CFL = 0.475.

The yield stress and viscosity values derived from the empirical correlations correspond to hyperconcentrated, clay-rich tailings mixtures (Table 1). The calculated yield stress and viscosity values for Aspen Pit 1 (τ_y = 249 kPa, η = 6,840 Pa·s) represent extremely high resistance, approaching paste-like conditions and far exceeding typical fluid tailings (Jeyapalan et al. 1983). This parameter set was selected to test the model's numerical stability under extreme rheological conditions rather than typical post-breach tailings behaviour. The Glenwood 1 parameters (τ_y = 797 Pa, η = 279 Pa·s) are more representative of concentrated fluid tailings flows.

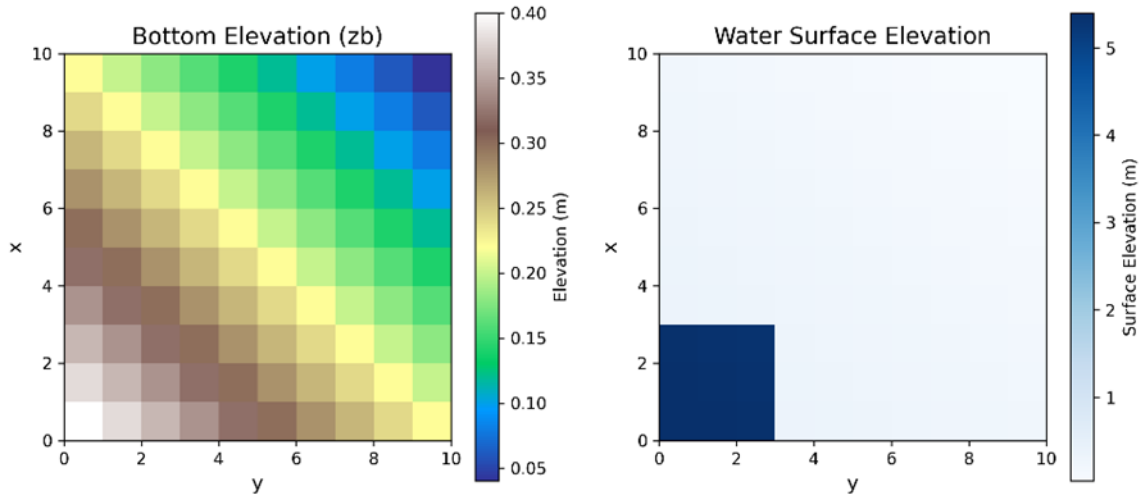

Figure 2 Initial model set-up conditions

Table 1 Dam break test tailings parameters

Parameter	Value		
	Newtonian	**Glenwood 1**	**Aspen Pit 1**
Manning n	0.04	0.04	0.04
Cv		0.5	0.55
ρ_m		2,650	2,750
K		2,285	2,285
α_1		0.0345	0.181
β_1		20.1	25.7
α_2		0.00283	0.0360
β_2		23.0	22.1

The gentle dual-direction gradient provides a realistic test for the well-balanced property of the solver, ensuring that both gravitational and topographic source terms are correctly integrated in 2 dimensions.

4 Results and discussion

4.1 Newtonian and non-Newtonian flow

The Newtonian frictionless case was first used to verify the accuracy of the numerical solver against the exact Riemann solution. The simulated depth and velocity fields reproduce the expected rarefaction and shock wave structure of the one-dimensional shallow-water problem extended to 2 dimensions. The advancing front develops sharply and maintains its form throughout the simulation, with no numerical oscillations.

The advancing front remains sharp throughout the simulation, with no evidence of spurious oscillations or numerical diffusion. The computed front position and maximum depth show good agreement with the analytical solution (Figure 3), confirming that the propagation is correctly resolved. This confirms the scheme's ability to accurately resolve discontinuities and maintain conservation of mass and momentum.

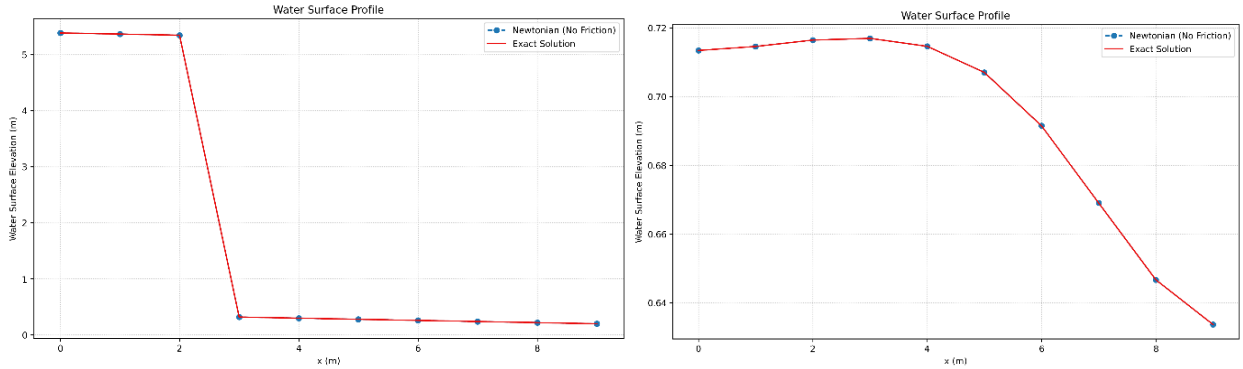

Figure 3 Comparison of the water elevation between Newtonian frictionless (blue dots) and Riemann exact solution (red line) for the Riemann problem test case at y index = 1

These results demonstrate that the finite-volume shock-capturing scheme with the Osher-type approximate Riemann solver accurately captures the essential dynamics of Newtonian shallow-water flow and provides a reliable baseline for the subsequent inclusion of frictional and rheological effects.

When bed friction was introduced using Manning's law, the flow response became more diffusive. The leading edge advanced more slowly, and the velocity field developed a smoother spatial gradient. The front position is slowed by approximately 10 to 15% compared to the frictionless run, while the maximum velocity decreases from 8.3 to 7.5 m/s. These differences align with theoretical expectations, as friction dissipates energy and redistributes. Importantly, the solver maintained stability and front resolution despite the additional source term (Figure 4).

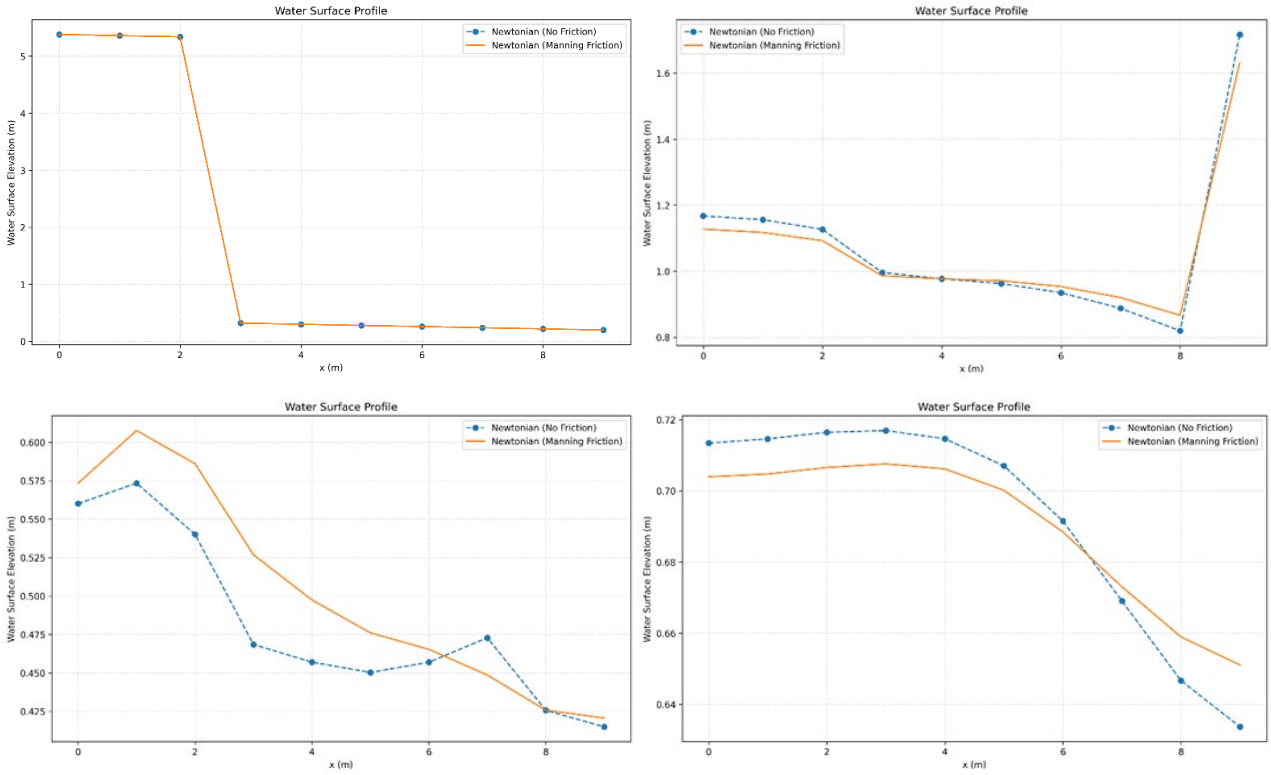

Figure 4 Comparison of the water elevation between Newtonian frictionless (blue line) and Newtonian with Manning friction (orange line) for the Riemann problem test case at y index = 1

4.2 Influence of rheology on flow dynamics

In the Glenwood 1 simulation, the flow remained mobile but exhibited greater resistance than the Newtonian case. The advancing front progressed downslope with a smoother, more rounded profile, and velocities were significantly reduced (Figure 5). This behaviour reflects the increased apparent viscosity, which damps turbulence and dissipates energy internally. This behaviour is consistent with previous laboratory studies of moderately concentrated mudflows, which show that mixtures with 45–50% solids retain mobility but exhibit strong shear thinning and internal damping (Coussot 2017; Iverson 1997; Major 1997). Physically, Glenwood 1 represents a transitional regime in which viscous and gravitational forces are in balance: the material still deforms under relatively small stresses, but inertia is no longer the dominant driver.

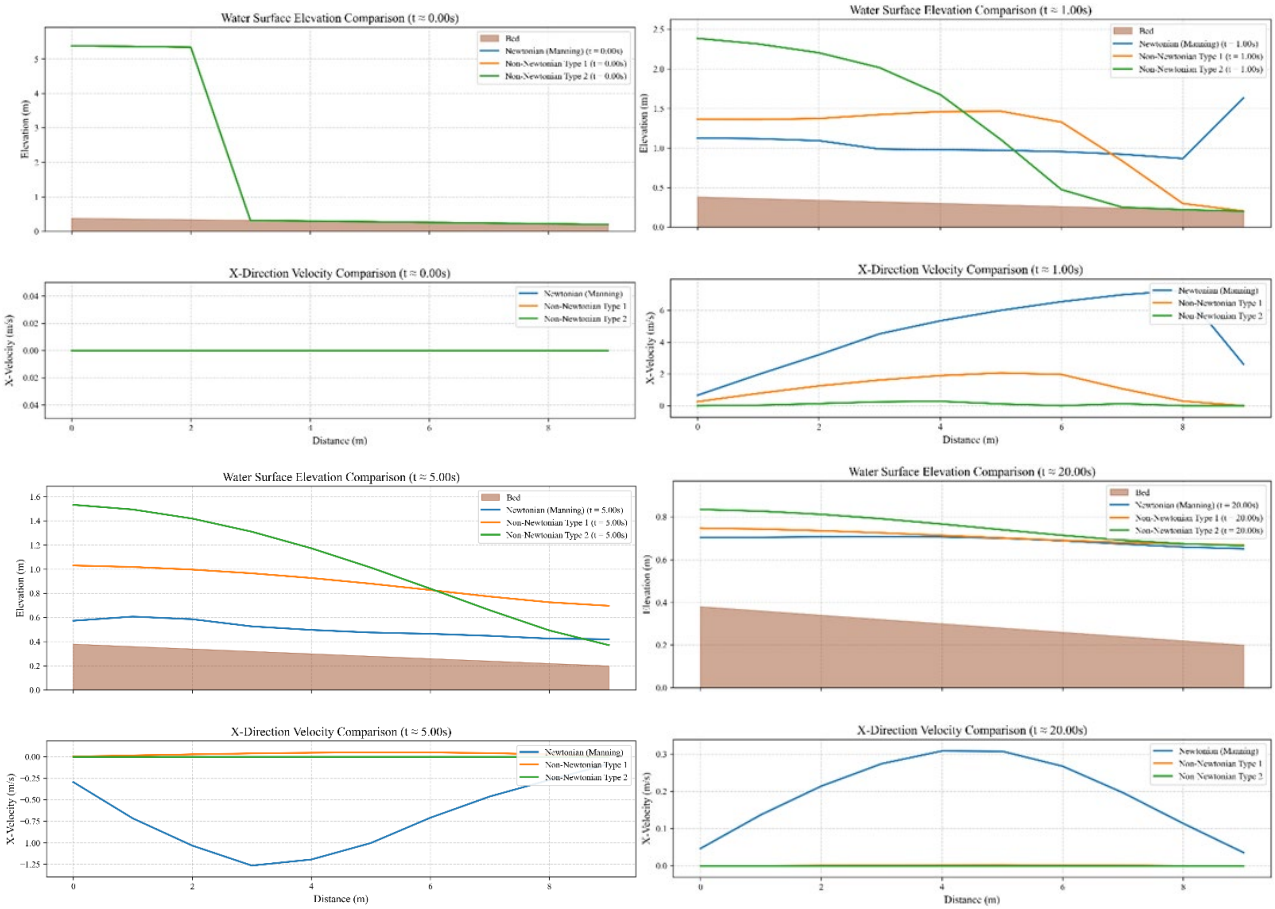

Figure 5 Comparison of the water elevation and velocity in the x direction between Newtonian with Manning friction (blue line) and the non-Newtonian Glenwood 1 (type 1, orange line), and the non-Newtonian Aspen Pit 1 (type 2, green line) for the Riemann problem test case at y index = 1

The Aspen Pit 1 case displayed a much stronger rheological effect. This mixture has a higher fraction of fine particles and clay minerals, which are known to increase both apparent viscosity and yield (Figure 5). The simulated flow advanced only a few metres before coming almost to rest. The flow surface thickened considerably near the source, and only a thin layer near the front showed any visible movement. This behaviour is characteristic of a yield-limited regime, where most of the material resists deformation, and motion is confined to narrow zones where shear stress exceeds the yield strength. Similar behaviour has been documented in laboratory and numerical studies of clay-rich debris flows and paste-like materials (Coussot & Piau 1994; Murillo & García-Navarro 2012; O'Brien et al. 1993; Takahashi 2007).

Table 2 summarises the maximum flow depth, total velocity, and wavefront position after one second for the Newtonian, Glenwood 1, and Aspen Pit 1 cases. The results clearly demonstrate the influence of rheology on flow mobility, the Newtonian case exhibits the highest velocity and front advancement, whereas the increasingly viscous and yield-limited Glenwood 1 and Aspen Pit 1 mixtures show a progressive reduction in

flow speed and runout, consistent with their higher apparent viscosities and yield stresses. As viscosity and yield stress increase, both velocity and runout decrease markedly, while flow thickness increases near the source.

Table 2 Comparison of maximum depth, maximum total velocity and wavefront position at t = 1 s

Parameter	Value		
	Newtonian	Glenwood 1	Aspen pit 1
Max depth (m)	1.6053	1.2240	2.0491
Max total velocity (m/s)	7.5055	2.3574	0.3485
Front position (m)	9.0	8.0	7.0

This sharp contrast between the 2 mixtures illustrates the strong sensitivity of flow dynamics to solids concentration and clay content. Numerous experimental studies confirm that even small increases in fine material can raise yield stress by one to 2 orders of magnitude (Coussot 2017; O'Brien et al. 1993; Sosio et al. 2007), leading to dramatic reductions in mobility. In other words, Aspen Pit 1 behaves as a paste-like, viscoplastic material, while Glenwood 1 remains a less-viscous fluid. Based on the relationship between clay content, yield stress, and flowability reported in tailings rheology studies (Parsons et al. 2001; Yang et al. 2020), Aspen mud resists deformation far more strongly and requires higher shear stresses to flow. The numerical model reproduces this behaviour well.

The solver handles both front thickening cases well without generating spurious oscillations or mass loss. This suggests that the numerical scheme is robust enough to handle the nonlinearity introduced by rheological stresses. The solver can smoothly transition between water-like and tailings-like flow regimes, a challenge that has been described in earlier incompressible flow implementations (Murillo & García-Navarro 2012).

In summary, these results show that even a simplified quadratic rheological model can capture the key physical differences between moderately viscous and yield-limited flows. Increasing viscosity and yield stress significantly reduce flow velocity and runout, leading to thicker, more stable deposits. This finding is directly relevant to predicting the behaviour of thickened tailings and debris flows, where material composition and particle size distribution strongly control mobility and hazard extent.

5 Conclusion

This study presents a depth-averaged incompressible flow solver that integrates an Osher-type Riemann solver with a quadratic viscoplastic rheological model suitable for concentrated sediment–water mixtures. The results lead to the following conclusions:

- The solver accurately reproduces Newtonian shallow-water dynamics, including rarefaction and shock waves, while maintaining mass and momentum conservation.
- The inclusion of bed friction introduces realistic energy dissipation without compromising numerical stability or front resolution.
- The quadratic rheological model successfully captures the transition from fluidised to yield-limited flow as apparent viscosity and yield stress increase.
- The numerical framework remains stable across a wide range of rheological regimes and resolves sharp fronts without spurious oscillations.

The simulations presented here focus on numerical verification and rheological sensitivity rather than event-specific calibration. Validation against laboratory experiments or documented tailings dam failures remains a critical next step but is currently constrained by limited availability of detailed rheological and time-resolved field data. The current model assumes a fixed bed ($\partial Z/\partial t = 0$). Real tailings flow entrains bed

material, particularly during the initial high-velocity phase, and deposits sediment progressively as shear rates decline. The total runout distance and final deposit geometry are strongly influenced by these processes (Iverson 2012; Pudasaini & Fischer 2020). Furthermore, the simulations were restricted to relatively short durations and small spatial domains. Longer simulations are required to investigate long-term runout and deposition/erosion.

Despite these limitations, the results demonstrate that the proposed framework offers a promising approach for simulating tailings dam break flows in a way that combines physically meaningful rheology with high-fidelity shock-capturing numerics.

Acknowledgement

This research is developed as part of the PhD project of the primary author and is funded by the Engineering and Physical Science Research Council (EPSRC) within the Geospatial Systems CDT (EPSRC Reference: EP/S023577/1), in partnership with Willis Towers Watson (WTW).

References

Azam, S & Li, Q 2010, 'Tailings dam failures: a review of the last one hundred years', *Geotechnical News Waste Geotechnics,* vol. 28, no. 4, pp. 50–53.

Bagnold, RA 1954, 'Experiments on a gravity-free dispersion of large solid spheres in a Newtonian fluid under shear', *Proceedings of the Royal Society of London. Series A. Mathematical and Physical Sciences*, The Royal Society, vol. 225, no. 1160, pp. 49–63, https://doi.org/10.1098/RSPA.1954.0186

Berthon, C & Michel-Dansac, V 2024, 'A fully well-balanced hydrodynamic reconstruction', *Journal of Numerical Mathematics*, vol. 32, no. 3, pp. 275–299, https://doi.org/10.1515/jnma-2023-0065

Brunner, GW 2016, *HEC-RAS River Analysis System User's Manual*, version 5.0, US Army Corps of Engineers, Davis, https://www.hec.usace.army.mil/software/hec-ras/documentation/hec-ras%205.0%20reference%20manual.pdf

Coussot, P & Piau, JM 1994, 'On the behavior of fine mud suspensions', *Rheologica Acta*, vol. 33, no. 3, pp. 175–184, https://doi.org/10.1007/BF00437302

Coussot, P 1997, *Mudflow Rheology and Dynamics*, Routledge, London, https://doi.org/10.1201/9780203746349

Dumbser, M, Toro, EF 2010, 'A simple extension of the Osher Riemann solver to non-conservative hyperbolic systems', *Journal of Scientific Computing*, vol. 48, no. 1, pp. 70–88, https://doi.org/10.1007/S10915-010-9400-3

FLO-2D Software Inc. 2004, *FLO-2D Reference Manual*, https://documentation.flo-2d.com/Build23/index.html

Ghahramani, N, Mitchell, A, Rana, NM, McDougall, S, Evans, SG & Take, WA 2020, 'Tailings-flow runout analysis: examining the applicability of a semi-physical area-volume relationship using a novel database', *Natural Hazards and Earth System Sciences*, vol. 20, no. 12, pp. 3425–3438, https://doi.org/10.5194/nhess-20-3425-2020

Ghahramani, N, Adria, DAM, Rana, NM, Llano-Serna, M, McDougall, S, Evans, SG & Take, WA 2024, 'Analysis of uncertainty and sensitivity in tailings dam breach-runout numerical modelling', *Mine Water and the Environment*, vol. 43, no. 1, pp. 87–103, https://doi.org/10.1007/S10230-024-00970-W

Glenis, V, Kutija, V & Kilsby, CG 2018, 'A fully hydrodynamic urban flood modelling system representing buildings, green space and interventions', *Environmental Modelling & Software*, vol. 109, pp. 272–292, https://doi.org/10.1016/j.envsoft.2018.07.018

Godunov, SK 1959, 'A finite difference method for the numerical computation of discontinuous solutions of the equations of fluid dynamics', *Matematicheskii Sbornik*, vol. 47(89) no. 3, pp. 271–306.

Harten, A 1983, 'High resolution schemes for hyperbolic conservation laws', *Journal of Computational Physics*, vol. 49, no. 3, pp. 357–393, https://doi.org/10.1016/0021-9991(83)90136-5

Iverson, RM 1997, 'The physics of debris flows', *Reviews of Geophysics*, vol. 35, no. 3, pp. 245–296, https://doi.org/10.1029/97RG00426

Iverson, RM 2012, 'Elementary theory of bed-sediment entrainment by debris flows and avalanches', *Journal of Geophysical Research Earth Surface*, vol. 117, no. F3, https://doi.org/10.1029/2011JF002189

Jeyapalan, JK, Duncan, JM & Seed, HB 1983, 'Analyses of flow failures of mine tailings dams', *Journal of Geotechnical Engineering*, vol. 109, no. 2, pp. 150–171, https://doi.org/10.1061/(ASCE)0733-9410(1983)109:2(150)

Julien, PY & Lan, Y 1991, 'Rheology of hyperconcentrations', *Journal of Hydraulic Engineering*, vol. 117, no. 3, pp. 346–53, https://doi.org/10.1061/(ASCE)0733-9429(1991)117:3(346)

Kheirkhah Gildeh, H, Halliday, A, Arenas, A & Zhang, H 2021, 'Tailings dam breach analysis: a review of methods, practices, and uncertainties', *Mine Water and the Environment*, vol. 40, no. 1, pp. 128–150, https://doi.org/10.1007/s10230-020-00718-2

Kheirkhah Gildeh, H, Sreekumar, U, Mohammadian, A, Nistor, I & Rennie, C 2024, 'Tailings dam breach assessment – a review', *Proceedings of International Mine Water Association Congress* 2024.

Lyu, Z, Chai, J, Xu, Z, Qin, Y & Cao, J 2019, 'A comprehensive review on reasons for tailings dam failures based on case history', *Advances in Civil Engineering*, vol. 1, no. 18, https://doi.org/10.1155/2019/4159306

Major, JJ 1997, 'Depositional processes in large-scale debris-flow experiments', *Journal of Geology*, vol. 105, no. 3, pp. 345–366, https://doi.org/10.1086/515930

Motsau, B, Van, D & Bench, W 2022, *Report on the Jagersfontein Tailings Disaster*, Bench Marks Foundation, Johannesburg https://www.bench-marks.org.za/wp-content/uploads/2022/10/Jagersfontein-report.pdf

Murillo, J & García-Navarro, P 2012, 'Wave Riemann description of friction terms in unsteady shallow flows: application to water and mud/debris floods', *Journal of Computational Physics*, vol. 231, no. 4, pp. 1963–2001, https://doi.org/10.1016/j.jcp.2011.11.014

Newland Bowker, L & Chambers, DM 2015, '*The risk, public liability, & economics of tailings storage facility failures'*, www.csp2.org

O'Brien, JS & Julien, PY 1988, 'Laboratory analysis of mudflow properties', *Journal of Hydraulic Engineering*, vol. 114, no. 8, pp. 877–887, https://doi.org/10.1061/(ASCE)0733-9429(1988)114:8(877)

O'Brien, JS, Julien, PY & Fullerton, WT 1993, 'Two-dimensional water flood and mudflow simulation', *Journal of Hydraulic Engineering*, vol. 119, no. 2, pp. 244–261, https://doi.org/10.1061/(ASCE)0733-9429(1993)119:2(244)

O'Brien, JS & Julien, PY 1985, 'Physical properties and mechanics of hyperconcentrated sediment flows', in DS Bowles (ed.), *Delineation of Landslide, Flash Flood, and Debris Flow Hazards in Utah*, Utah Water Research Laboratory, Logan, pp. 260–280.

Parsons, JD, Whipple, KX & Simoni, A 2001, 'Experimental study of the grain flow, fluid-mud transition in debris flows', *Journal of Geology*, vol. 109, no. 4, pp. 427–447, https://doi.org/10.1086/320798

Piciullo, L, Storrøsten, EB, Liu, Z, Nadim, F & Lacasse, S 2022, 'A new look at the statistics of tailings dam failures', *Engineering Geology*, vol. 303, https://doi.org/10.1016/j.enggeo.2022.106657

Pudasaini SP, Fischer JT 2020, 'A mechanical erosion model for two-phase mass flows', *International Journal of Multiphase Flow*, vol. 132, https://doi.org/10.1016/j.ijmultiphaseflow.2020.103416

Rana, NM, Ghahramani, N, Evans, SG, McDougall, S, Small, A & Take, WA 2021, 'Catastrophic mass flows resulting from tailings impoundment failures', *Engineering Geology*, vol. 292, https://doi.org/10.1016/j.enggeo.2021.106262

Rico, M, Benito, G & Díez-Herrero, A 2008, 'Floods from tailings dam failures', *Journal of Hazardous Materials*, vol. 154, no. 1–3, pp. 79–87, https://doi.org/10.1016/J.JHAZMAT.2007.09.110

Sosio, R, Crosta, GB, & Frattini, P 2007, 'Field observations, rheological testing and numerical modelling of a debris-flow event', *Earth Surface Processes and Landforms*, vol. 32, no. 2, pp. 290–306, https://doi.org/10.1002/ESP.1391

Takahashi, T 2007, *Debris Flow: Mechanics, Prediction and Countermeasures*, Taylor & Francis, London, https://doi.org/10.1201/9780203946282

Toro, EF 2001, *Shock-Capturing Methods for Free-Surface Shallow Flows*, Wiley, Chichester.

Wang, K, Yang, P, Yu, G, Yang, C & Zhu, L 2020, '3D numerical modelling of tailings dam breach run out flow over complex terrain: a multidisciplinary procedure', *Water 2020,* vol. 12, no.3, pp. 25–38, https://doi.org/10.3390/W12092538

Yang, K, Xu, ZM, Tian, L, Wang, K, Ren, Z, Tang, YJ, Luo, JY & Gao, HY 2020, 'Significance of coarse clasts in viscous debris flows', *Engineering Geology*, vol. 272, https://doi.org/10.1016/J.ENGGEO.2020.105665

Zhu, F, Zhang, W & Puzrin, AM 2024, 'The slip surface mechanism of delayed failure of the Brumadinho tailings dam in 2019', *Communications Earth and Environment*, vol. 5, no. 1, https://doi.org/10.1038/s43247-023-01086-9